NASA

Predicting Turbulent Convective Heat Transfer in Three-Dimensional Duct Flows

M. Rokni
Lund Institute of Technology, Lund, Sweden

T. B. Gatski
Langley Research Center, Hampton, Virginia

December 1999

Predicting Turbulent Convective Heat Transfer in Three-Dimensional Duct Flows

M. Rokni

Division of Heat Transfer

Lund Institute of Technology, 221 00 Lund, Sweden

T. B. Gatski

Computational Modeling & Simulation Branch

NASA Langley Research Center, Hampton, VA 23681, USA

Abstract

The performance of an explicit algebraic stress model is assessed in predicting the turbulent flow and forced heat transfer in straight ducts, with square, rectangular, trapezoidal and triangular cross sections, under fully developed conditions over a range of Reynolds numbers. Iso-thermal conditions are imposed on the duct walls, and the turbulent heat fluxes are modeled by gradient-diffusion type models. At high Reynolds numbers ($\gtrsim 10^5$), wall functions are used for the velocity and temperature fields, while at low Reynolds numbers, damping functions are introduced into the models. Hydraulic parameters such as friction factor and Nusselt number are well predicted, even when damping functions are used, and the present formulation imposes minimal demand on the number of grid points without any convergence or stability problems. Comparison between the models is presented in terms of the hydraulic parameters, friction factor and Nusselt number, as well as in terms of the secondary flow patterns occurring within the ducts.

1. Introduction

The performance of a turbulence model in predicting the velocity and temperature fields of relevant industrial problems has become increasingly important during the last few years. This improved predictive performance is also true for turbulent duct flow, which occurs frequently in many industrial applications, such as compact heat exchangers, gas turbine cooling systems, cooling channels in combustion chambers, nuclear reactors, and others. The cross section of these ducts might be both orthogonal (square or rectangular) and nonorthogonal (such as trapezoidal), in which the generated flow is extremely complex. Sometimes, the ducts are also wavy or corrugated in the streamwise direction and might be manufactured with ribs to achieve faster transition to turbulence.

Several fundamental studies of turbulent flow in square and rectangular ducts exist in the literature. Direct numerical simulations have been carried out for a square duct by Gavrilakis (1992) and Huser and Biringen (1993) with Reynolds numbers of 4410 and $\approx 10^4$, respectively. Large eddy simulations for square and rectangular ducts have been reported by Madabhushi and Vanka (1991) at a Reynolds number of 5800, and by Su and Friedrich (1994) and Meyer and Rehme (1994) at Reynolds numbers up to 4.9×10^4. Nevertheless, limitations on computational power and memory make it

almost impossible to directly solve for the turbulent flow field in practical engineering duct flows using a direct numerical simulation (DNS) approach for the foreseeable future. Large eddy simulations (LES) may be more tractable; although to date, their use has not been widespread. Thus, the prediction of the flow and heat transfer characteristics in engineering duct flows still requires a Reynolds-averaged approach using suitable turbulent closure models for both the velocity and temperature fields.

It is known that secondary motions take place in the corner of noncircular straight ducts in the plane perpendicular to the streamwise flow direction. These motions are turbulence-induced and are commonly referred to as motions of Prandtl's second kind. Such motions are of importance since they redistribute the kinetic energy, influence the streamwise velocity, and thereby affect the wall shear stress and heat transfer. The effect of secondary motions of Prandtl's second kind on the wall shear stresses and heat fluxes increases considerably when the ducts are corrugated. A linear eddy viscosity model (LEVM) does not have the ability to predict secondary flows, but still it is one of the most popular models among engineers owing to its simplicity and overall good performance properties. Previously, Rokni and Sundén (1996, 1998) employed a nonlinear eddy viscosity model (NLEVM) for predicting the flow and heat fluxes in straight and wavy ducts with trapezoidal cross sections. This level of closure accounts for the Reynolds stress anisotropy and is then able to predict the secondary flows within the relative cost of a two-equation formulation.

In the study reported here, the earlier work of Rokni and Sundén (1996, 1998) is extended to arbitrary ducts by using an explicit algebraic stress model (EASM). The method is applied to square, rectangular, trapezoidal, and triangular ducts with iso-thermal wall conditions using gradient-diffusion type heat flux models. The heat flux models are a simple eddy diffusivity model (SED), a generalized gradient diffusion hypothesis (GGDH) model, and a model extracted from the empirical WET hypothesis (Launder 1988). The EASM representation is used for both low- and high-Reynolds numbers without introducing any damping functions into the tensor representation for the Reynolds stresses; however, at low Reynolds numbers, damping functions are introduced into the isotropic eddy viscosity and the heat flux models. At high Reynolds numbers ($\gtrsim 10^5$), wall functions are used for both the velocity and temperature fields. Jayatilleke's P-function (1969) is not used because it is shown to be a main source of error if wall functions are used for (numerically) predicting the friction factor in ducts.

One difficulty associated with turbulent convective heat transfer and fluid flow in ducts is obtaining satisfactory results for both friction factor and Nu-number, if wall functions are used. Usually, either friction factor or Nu-number can be predicted satisfactorily, but not both of them. Another problem with using wall functions in complex geometry (duct) flows is the variability of the minimum y^+ value along the grid line adjacent to the boundary. (See, e.g., Rokni and Sundén, 1996.) Uniformity can be achieved by setting the grid points adjacent to the wall in certain positions; however, while this placement is easily done in orthogonal geometries, it is extremely difficult in nonorthogonal geometries. Alternatively, low-Reynolds number versions of the models usually cannot be extended to Reynolds numbers $\gtrsim 10^4$ based on hydraulic diameter (see e.g., Rokni and Sundén, 1999b). Therefore, it is desirable to develop a

2

model that not only predicts these hydraulic parameters satisfactorily, but that also can be used for a very wide range of Reynolds numbers with less demand on the number of grid points and without any convergence problem.

2. Mean and Turbulent Equations

A Reynolds-averaged Navier-Stokes (RANS) approach is used to predict the fully developed turbulent flow and heat transfer in the three-dimensional duct flow. The governing equations for the mean and turbulent quantities are

$$\frac{\partial \rho}{\partial t} + \frac{\partial}{\partial x_j}(\rho U_j) = 0, \tag{1}$$

$$\frac{\partial \rho U_i}{\partial t} + \frac{\partial}{\partial x_j}(\rho U_i U_j) = -\frac{\partial P}{\partial x_i} + \frac{\partial}{\partial x_j}\left[\mu\left(\frac{\partial U_i}{\partial x_j} + \frac{\partial U_j}{\partial x_i}\right)\right] + \frac{\partial}{\partial x_j}(-\rho\overline{u_i u_j}), \tag{2}$$

$$\frac{\partial(\rho T)}{\partial t} + \frac{\partial}{\partial x_j}(\rho U_j T) = \frac{\partial}{\partial x_j}\left[\frac{\mu}{Pr}\frac{\partial T}{\partial x_j}\right] + \frac{\partial}{\partial x_j}(-\rho\overline{u_j t}), \tag{3}$$

The turbulent stresses $\rho \tau_{ij}$ $(= -\rho\overline{u_i u_j})$ and turbulent heat fluxes $(\rho c_p \overline{u_j t})$ require modeling in order to close the equations.

For the modeling of the Reynolds stresses $\rho \tau_{ij}$, within the context of an algebraic stress formulation, transport equations for the turbulent kinetic energy and turbulent dissipation rate are needed:

$$\frac{\partial \rho k}{\partial t} + \frac{\partial}{\partial x_j}(\rho U_j k) = \frac{\partial}{\partial x_j}\left[\left(\mu + \frac{\mu_t}{\sigma_k}\right)\frac{\partial k}{\partial x_j}\right] + P_k - \rho\varepsilon. \tag{4}$$

$$\frac{\partial \rho \varepsilon}{\partial t} + \frac{\partial}{\partial x_j}(\rho U_j \varepsilon) = \frac{\partial}{\partial x_j}\left[\left(\mu + \frac{\mu_t}{\sigma_\varepsilon}\right)\frac{\partial \varepsilon}{\partial x_j}\right] + C_{\varepsilon 1}\frac{\varepsilon}{k}P_k - f_2 C_{\varepsilon 2}\rho\frac{\varepsilon^2}{k}. \tag{5}$$

where $P_k = \rho\tau_{ij}\partial U_i/\partial x_j$ is the production term. The constants $C_{\varepsilon 1}$ and $C_{\varepsilon 2}$ are set to 1.44 and 1.83, respectively, and the turbulent eddy viscosity is calculated as $\mu_t = \rho f_\mu C_\mu \frac{k^2}{\varepsilon}$ where $C_\mu \approx 0.09$. The functions f_1, f_2, and f_μ are damping functions and are equal to unity in the fully turbulent region. In this study, the Abe-Kondoh-Nagano (1995) formulations for f_1, f_2, and f_μ are used and are given by

$$f_2 = \left(1 - e^{-\frac{y^+}{3.8}}\right)^2\left[1 + 0.15e^{-\left(\frac{Re_t}{3.5}\right)^2}\right], \quad f_\mu = \left(1 - e^{-\frac{y^+}{16}}\right)^2\left[1 + \frac{5}{(Re_t)^{0.75}}e^{-\left(\frac{Re_t}{200}\right)^2}\right] \tag{6}$$

where

$$y^+ = u_\varepsilon\frac{\rho d}{\mu} = \left(\frac{\mu\varepsilon}{\rho}\right)^{0.25}\frac{\rho d}{\mu}, \qquad Re_t = \frac{\rho k^2}{\mu\varepsilon}, \tag{7}$$

and d is the normal distance to the nearest wall. When the AKN model is used, the constants σ_k and σ_ε are both set to 1.4, and all the remaining constant coefficients are calibrated against the DNS channel flow data of Kim et al. (1987). At high Reynolds numbers, $\sigma_k = 1$ and σ_ε is determined from $\kappa^2/[\sqrt{C_\mu}(C_{\varepsilon 2} - C_{\varepsilon 1})]$.

3

The explicit algebraic stress model used is an extension of the Gatski and Speziale (1993) model and is described in Rumsey et al. (1999). In terms of the turbulent stress anisotropy b_{ij}, it can be written as

$$b_{ij} = \frac{\tau_{ij}}{2k} - \frac{\delta_{ij}}{3} = \alpha_1 S_{ij} + \alpha_2 (S_{ik}W_{kj} - W_{ik}S_{kj}) + \alpha_3\left(S_{ik}S_{kj} - \frac{1}{3}\{\mathbf{S}^2\}\delta_{ij}\right), \quad (8)$$

where S_{ij} and W_{ij} are the mean strain rate and rotation rate tensors, respectively $(S_{ij} + W_{ij} = \partial U_i/\partial x_j)$. The α_i's are scalar coefficient functions of the invariants $\eta^2 (= S_{ij}S_{ij} = \{\mathbf{S}^2\})$ and $\xi^2 (= W_{ij}W_{ij} = -\{\mathbf{W}^2\})$, and are given by

$$\alpha_1^3 - \frac{\gamma_1}{\gamma_0\eta^2\tau}\alpha_1^2 + \frac{1}{4\gamma_0^2\eta^4\tau^2}\left[\gamma_1^2 - 2\alpha_1\eta^2\tau^2\gamma_0 - 2\eta^2\tau^2\left(\frac{a_3^2}{3} - \mathcal{R}^2 a_2^2\right)\right]\alpha_1 + \frac{a_1\gamma_1}{4\gamma_0^2\eta^4\tau} = 0 \tag{9}$$

$$\alpha_2 = a_4 a_2\alpha_1 \quad \text{and} \quad \alpha_3 = -2a_4 a_3\alpha_1 \tag{10}$$

where

$$a_1 = 0.487, \quad a_2 = 0.80, \quad a_3 = 0.375, \quad a_4 = g\tau, \quad \tau = \frac{k}{\varepsilon} \tag{11}$$

$$\mathcal{R} = \frac{\xi^2}{\eta^2}, \quad g = \left[\gamma_1 - 2\gamma_0\alpha_1\eta^2\tau\right]^{-1}, \quad \gamma_0 = 1.19 \text{ and } \gamma_1 = 0.7. \tag{12}$$

The proper choice for α_1 is the minimum real root of Eq. (9) (Jongen and Gatski 1999).

Three different models are used to provide closure for the turbulent heat flux term. The first is an isotropic, simple eddy diffusivity (SED) model based on the Boussinesq approximation,

$$\overline{u_j t} = -\frac{\mu_t}{\rho\sigma_T}\frac{\partial T}{\partial x_j} \tag{13}$$

where the turbulent Prandtl number for temperature σ_T is set to 0.89. The second is a model based on a generalized gradient diffusion hypothesis (GGDH),

$$\overline{u_j t} = -C_t\frac{k}{\varepsilon}\left(\overline{u_j u_k}\frac{\partial T}{\partial x_k}\right), \tag{14}$$

and the third model is based on the WET method and is given by

$$\overline{u_j t} = -C_t\frac{k}{\varepsilon}\left(\overline{u_j u_k}\frac{\partial T}{\partial x_k} + \overline{u_k t}\frac{\partial U_j}{\partial x_k}\right), \tag{15}$$

where $C_t = 0.3$ in both the GGDH and the WET models. At low Reynolds numbers, a damping function for the SED model (f_μ) is included in the turbulent eddy viscosity μ_t, and for the GGDH and WET models, a damping function $f_{\mu T}$ is introduced. This damping function is a Lam-Bremhorst (LB) (1981) type model which is given by

$$f_{\mu T} = \left(1 - e^{-0.0225 Re_k}\right)^2\left(1 + \frac{41}{Re_t}\right), \tag{16}$$

4

where $Re_k = \rho\sqrt{k}d/\mu$. If the same number of grid points was used in the cross section, it was found that using the LB model in the GGDH and WET closures gave better results than the AKN model for flows where $Re > 10^4$. Note that the WET model is implicit, and the resulting system of equations for the heat fluxes are solved analytically in each iteration (no numerical inner iteration loop).

Both friction factor and Nusselt number have been obtained from the computations. The calculated friction factor is thus related to the Prandtl-law (Incropera and DeWitt 1996) as

$$\frac{1}{\sqrt{4f}} = 2\log\left(Re\sqrt{4f}\right) - 0.8. \tag{17}$$

The Re number is based on the hydraulic diameter defined for two or three walls as

$$D_h = \frac{4A_{\text{cross}}}{a + \frac{h}{\sin\phi}} \quad \text{or} \quad D_h = \frac{4A_{\text{cross}}}{a + b + \frac{h}{\sin\phi}}, \tag{18}$$

where a, b, h, and ϕ are base length, upper length, height, and base angle, respectively. The reference to two or three walls is to the number of walls in the cross section when symmetry conditions are used, and A_{cross} is the cross-section area which can be defined as $0.5(a + h)$ for all cases considered here.

The calculated Nu-number is related to the Dittus-Boelter correlation (Incropera and DeWitt 1996) by

$$Nu = 0.023Re^{0.8}Pr^{0.3} \quad \text{for} \quad Re \gtrsim 8000 \tag{19}$$

At high Reynolds numbers, the law of the wall is assumed to be valid for both the velocity and temperature fields in the near wall region (see Rokni and Sundén (1996, 1999a) for implementation details). While the log-law behavior is assumed for the velocity field, the temperature field can be treated by either of two methods. One is the usual log-law behavior, and the other is the commonly used P-function (Jayatilleke, 1969) method. By using the latter approach, the temperature field is given by

$$T^+ = \frac{(T_w - T_p)\rho c_p U^+}{q_w} = \sigma_T\left[U^+ + P\left(\frac{Pr}{\sigma_T}\right)\right] \tag{20}$$

where the P-function can be expressed as

$$P\left(\frac{Pr}{\sigma_T}\right) = 9.24\left[\left(\frac{Pr}{\sigma_T}\right)^{0.75} - 1\right]\left[1 + 0.28e^{\left(-0.007\left(\frac{Pr}{\sigma_T}\right)\right)}\right], \tag{21}$$

and $\sigma_T = 0.89$. This method is very popular, especially in commercial codes; however, two disadvantages of the method in duct flows are that the temperature field will be directly dependent on the velocity field, and that the von Karman constant κ may play a significant roll in the determination of the Nu-number. Figure 1 clearly shows the effect of the κ value on the calculated friction factor and Nu-number in a square duct (using the EASM and the SED model). A question that now arises is which value of the von Karman constant should be chosen. A value of $\kappa = 0.408$ gives the best result for the friction factor; $\kappa = 0.46$ gives the best result for the Nu-number.
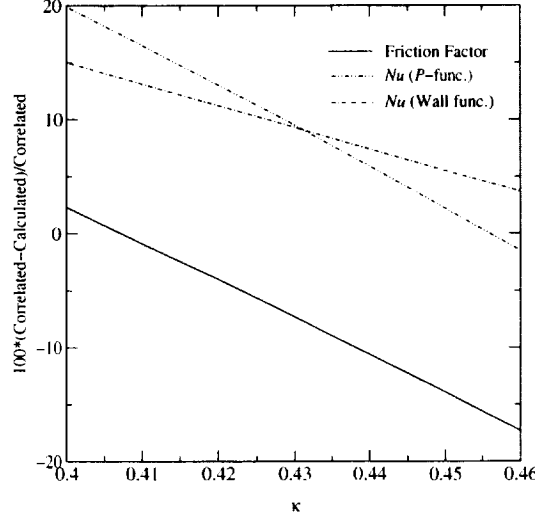
Figure 1. Calculated friction factor and Nu-number compared with experimental correlations in a square duct using EASM, SED, and two near wall treatments for the temperature field.

Rokni and Sundén (1996) assumed an average value of $\kappa = 0.435$. In light of this ambiguity, the former approach of assuming a log-law behavior for the temperature field will be used here.

The numerical method is based on the finite volume technique, with a nonstaggered grid arrangement. The SIMPLEC algorithm is used for pressure-velocity coupling. A modified SIP method is implemented for solving the equations. The QUICK scheme is used for treating the convective terms in the momentum equation. However, to achieve stability in the k and ε equations, a hybrid scheme is used for the convective terms. A further discussion of the specification and implementation of the boundary conditions, as well as the numerical procedure used in the solution of the mean and turbulent equations, can be found in Rokni and Sundén (1996, 1999b).

3. Results

Straight ducts with square, rectangular, and trapezoidal cross sections, and a wavy duct are considered in this investigation. Only one quarter of the duct with square and rectangular cross sections and only half of the duct with a trapezoidal cross section are considered by imposing symmetry conditions. Sketches of the various duct configurations are shown in Fig. 2. The calculations focus on fully developed, three-dimensional, turbulent duct flow. Results of mean velocity, and friction factor and Nu-number distributions are presented, the latter two quantities being the most important hydraulic parameters from an engineering standpoint. In addition, the secondary flow generated within the ducts is also analyzed.
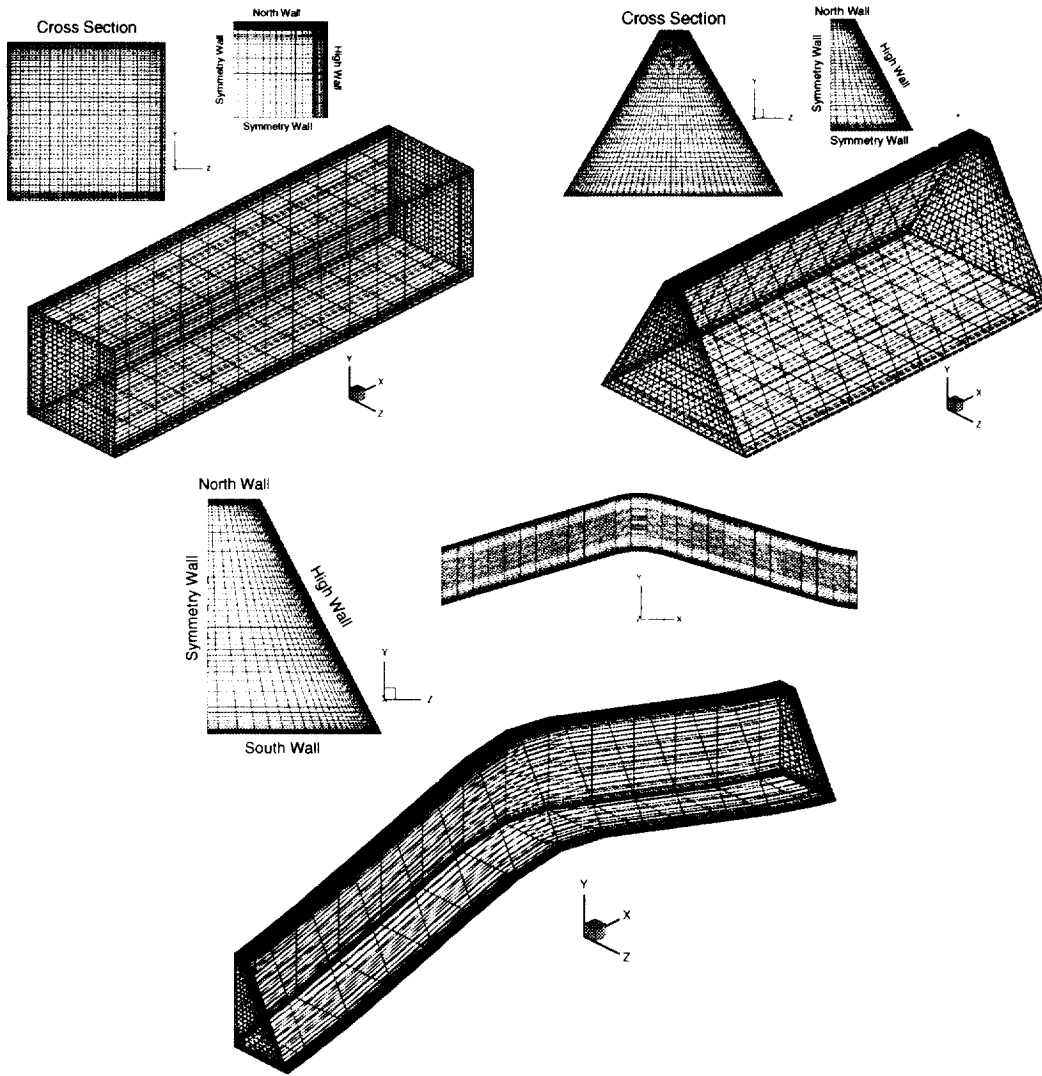
6

Figure 2. Ducts under consideration.

3.1 Grid Sensitivity

A nonuniform grid distribution is employed in the plane perpendicular to the main flow direction. Close to each wall, the number of grid points or control volumes are increased to enhance the resolution and accuracy. From the duct center to each wall, the grid distance is multiplied by a stretching factor (ST) less than unity. Thus, the smaller this factor, the more grid points are concentrated near the wall (i.e., finer grid near wall). A different number of grid points was used in the cross-sectional plane in order to establish the accuracy of the calculations. Table 1 shows the calculated Nu-number and friction factor in a square duct with different stretching factors and number of grid points, when using the EASM. The calculated Nu-number (by GGDH) and friction factor are compared with the correlations mentioned in previous sections. In the table, Nu_{DB} stands for Nu-number calculated from the Dittus-Boelter correlation, and f_{Pr} stands for friction factor calculated from the Prandtl-law correlation.

As is evident from Table 1, decreasing the stretching factor (inserting more grid points in the viscous sublayers) for a specific number of grid points increases the accuracy of the calculations. For example, using 31×31 grid points with stretching factor 0.85 yields predictions as accurate as 35×35 number of grid points with a stretching factor of 0.9. In this study, 31×31 grid points in the cross section with different stretching factors (depending on the Re number) has been used. If wall functions

Table 1. Calculated friction factor and Nu-number for a square duct with different numbers of grid points and stretching factors using low Reynolds version.

ST	Grid	Re	$f \times 10^3$	$f_{\mathrm{Pr}} \times 10^3$	diff %[a]	GGDH	Nu_{DB}	diff %[a]
0.9	21×21	4561	10.098	9.602	-5.2	16.3	17.6	7.4
0.9	31×31	4588	9.981	9.586	-4.1	16.2	17.7	8.5
0.9	35×35	4603	9.915	9.576	-3.5	16.2	17.8	8.9
0.9	41×41	4615	9.864	9.569	-3.1	16.2	17.8	9.0
0.9	51×51	4619	9.847	9.567	-2.9	16.2	17.8	9.0
0.93	31×31	4549	10.154	9.610	-5.7	16.6	17.3	4.0
0.85	31×31	4604	9.912	9.576	-3.5	16.3	17.8	8.4
0.85	41×41	4607	9.900	9.574	-3.4	16.3	17.8	8.4

[a]diff % $= 100 \times$ (correlated - calculated)/correlated

were used ($Re > 10^4$ based on hydraulic diameter), 21×21 to 31×31 (depending on the Re number) grid points were sufficient to obtain reasonable accuracy for both the friction factor and Nu-number in the square ducts.

3.2 Square Duct

The square duct is the least complicated geometry to be studied here. The flow and heat transfer results presented here show the wide range of Reynolds numbers over which the current formulation can be successfully used.

3.2.1 Secondary Flow Patterns

In Fig. 3, the secondary flow pattern (velocity vectors) in the fully developed region of a square duct is shown at a Reynolds number near 4800. The results predicted by the EASM (with damping functions) are in excellent qualitative agreement with the DNS study of Mompean et al. (1996) and Gavrilakis (1992). Similar secondary flow patterns are predicted at both the low and high Reynolds numbers considered.

As is well known, in laminar flow these secondary motions do not occur. In turbulent flow, the forces driving the secondary motion are concentrated in the region close to each corner. These motions are generated by gradients of the normal turbulent stresses. However, the linear $k - \varepsilon$ model (LEVM) (see e.g., Rokni, 1998) does not correctly predict these secondary motions because of its inability to accurately account for the individual normal Reynolds stresses $\overline{u_i u_i}$. The LEVM yields
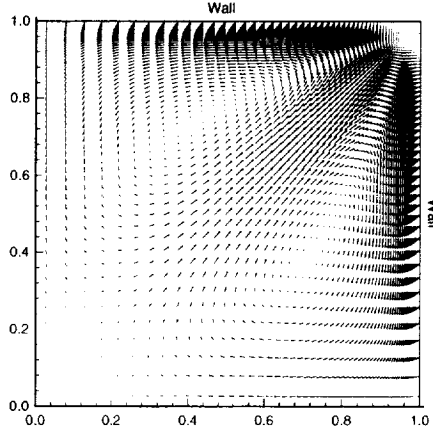
8

Figure 3. Predicted secondary motion velocity vectors in a square duct for Re near 4800.

the physically incorrect expression $\overline{uu} = \overline{vv} = \overline{ww}$. It is worthwhile to point out that secondary motions are found with LEVM; however, they are extremely small, about $10^{-4}\%$ to $10^{-3}\%$ of the streamwise flow, and cannot normally be detected. These very small motions lie in the limit of numerical/computer accuracy (absolute values of $10^{-6} - 10^{-7}$). While the redistribution of the turbulent kinetic energy into the normal components of the Reynolds stresses is important in correctly predicting the secondary flow pattern, it is equally important that the Reynolds shear stress component be accurately predicted. The turbulent shear stress is the essential element in the production of the turbulent kinetic energy and as such determines the overall turbulent energy level of the flow.

The predicted secondary velocity profile using the EASM, combined with both the wall functions ($Re = 7.1 \times 10^4$) and damping functions ($Re = 5600$), is shown in Fig. 4. (Since the velocity vectors in the low Re case are smaller than in the high Re case, the results from the low Re case have been magnified ($\times 10$) for easier comparison of the corresponding flow patterns.) In both Reynolds number cases, the secondary motions consist of two counter-rotating vortices which transport high momentum fluid towards the duct corner along the bisector and then outwards along the walls. The difference between the two Reynolds numbers lies in the spatial extent of the vortices within the duct.

At low Reynolds numbers, the secondary flow close to the duct center is weak, and its influence on the streamwise flow is small; however, the secondary motions concentrated near the duct corners are strong and their effect on the streamwise flow is large (see Fig. 5). Nevertheless, even with the existence of the two counter-rotating vortices, very close to the corner, a small region of stagnant flow exists. Such a region is an artifact of the symmetric structure of the counter-rotating vortices in the square duct. As will be seen in the results from the more complicated duct geometries to be analyzed, such a symmetric structure no longer exists, and the corner flow pattern
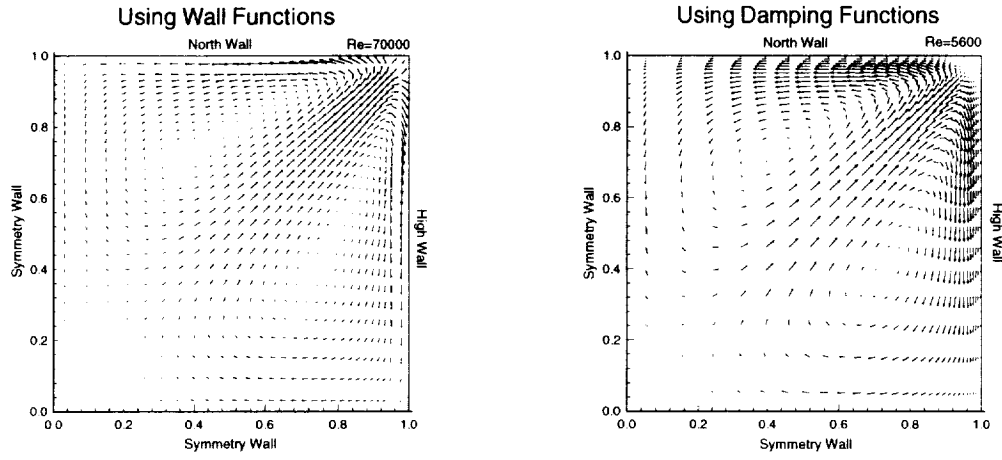
9

Figure 4. Secondary motion velocity vectors predicted by the EASM with different near-wall treatments.

is more complicated. Figure 5 shows the effect on the streamwise velocity contours (U/U_{bulk}) predicted by the EASM using both the wall function and damping function approach. As can be seen for the high Reynolds number case, using wall functions rather than damping functions increases the predicted streamwise velocity along the corner bisector toward the corner.
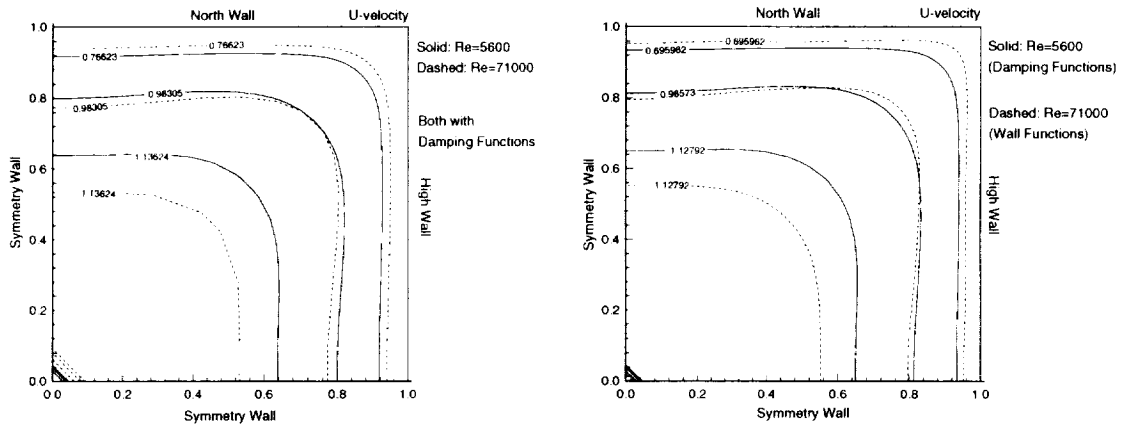

Figure 5. Predicted streamwise velocity contours using EASM at two different Reynolds numbers and using different near-wall treatments.

3.2.2 Hydraulic Parameters

The accurate prediction of the friction factor and Nu-number is an important consideration in assessing turbulent model performance. In this subsection, the results of the computations using both wall functions and damping functions are presented.

10

The calculated friction factor and Nu-number at high Reynolds numbers using wall functions are shown in Fig. 6. The friction factor obtained from the EASM is in excellent agreement with the Prandtl-law correlation. However, the model could not be applied for Re numbers less than about 2.0×10^4 due to the large distance between the wall and the nearest adjacent points.

Both the GGDH and WET methods are in excellent agreement with the Dittus-Boelter correlation (less than 3% deviation), while the SED method deviates somewhat more from this correlation (see Fig. 6). The GGDH and WET models could not be applied for Re number less than about 2.0×10^4 without additional numerical manipulations, e.g., using the results from a higher Re number as input data for the lower Re number.
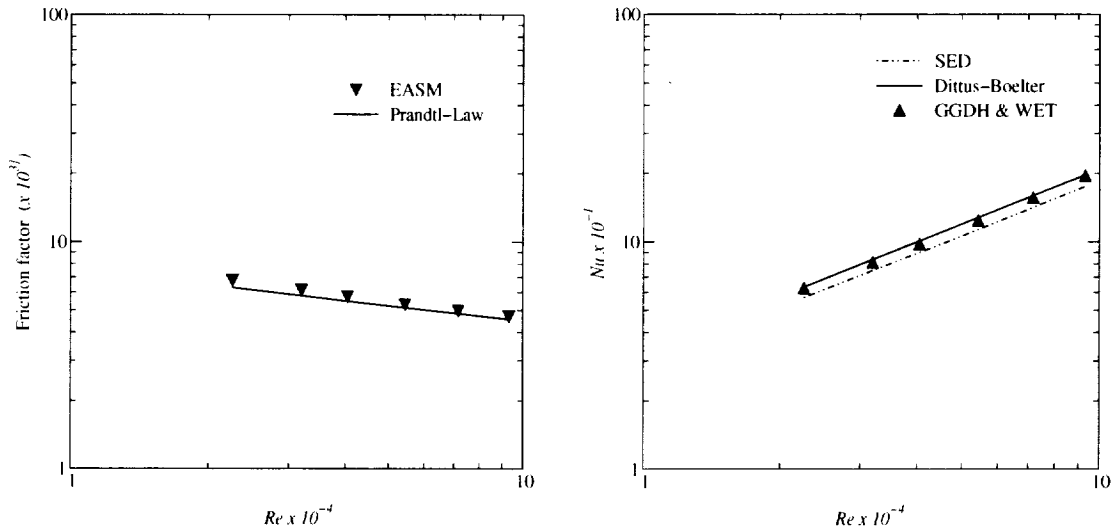

Figure 6. Calculated friction factor and Nu-number using the EASM with the wall functions.

One problem associated with using the wall functions is that the grid points adjacent to a wall should be a certain distance away from the nearest wall, to get the average y^+ value in an acceptable range ($y^+ > 35$; see Fig. 4). The problem is more evident when the ducts are wavy and/or have trapezoidal cross sections. This problem can be alleviated by using the EASM presented here. Nevertheless, the damping function requirement of calculating the normal distance from any point to the nearest wall is not an easy task in general geometries.

Figure 7 shows that the calculated friction factor using the EASM is able to captures the Prandtl-law correlation (about 5% over-predicted). The figure also shows that the Nu-number, obtained from the GGDH and WET methods, agrees rather well with the Dittus-Boelter correlation, while the SED method gives less accurate results. It should be mentioned that the GGDH and WET models underpredict the Dittus-Boelter correlation for Re numbers less than about 8000. The experimental work of Lowdermilk et al. (1969) also shows that the Nu-number in square ducts
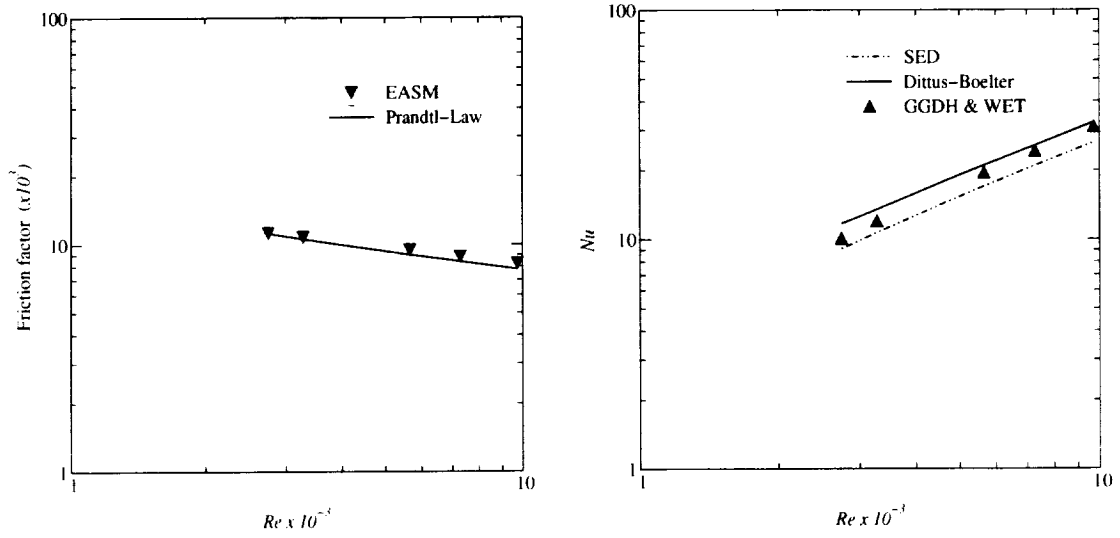
11

Figure 7. Calculated friction factor and Nu-number using the EASM and damping functions.

underpredicts from the Dittus-Boelter equation for Re numbers less than about 8000.

The presented calculation procedure is highly stable and can be extended to a much higher Re number than 10^4 with a minimal demand on the number of grid points. In Fig. 8, the calculations were performed with only 31×31 grid points for all Reynolds numbers. No convergence problems arose even at very high Re
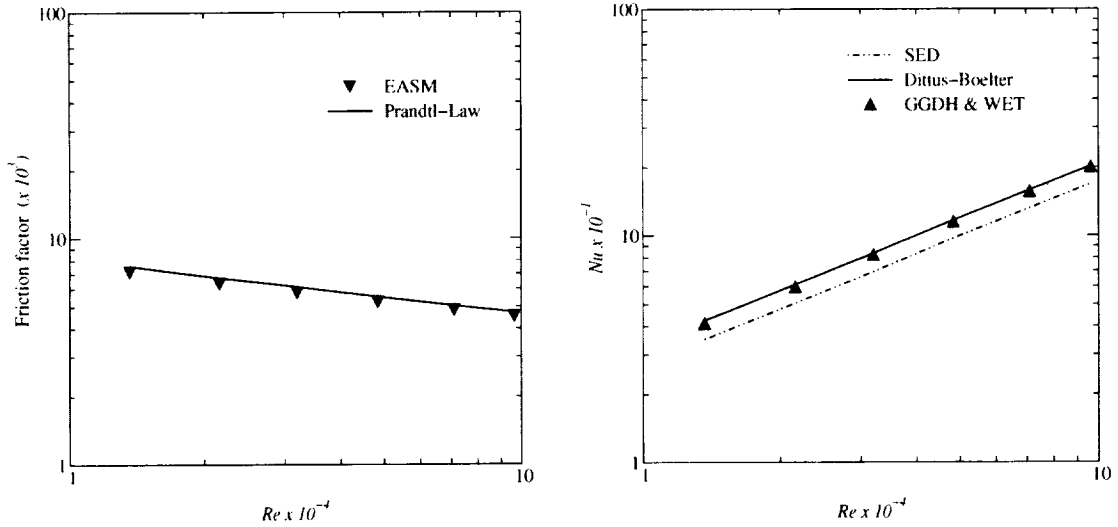

Figure 8. Calculated friction factor and Nu-number using the EASM with damping functions at high Re numbers.

numbers by using the present models. The friction factor obtained from the EASM is over-predicted by about 5% compared to the Prandtl-law correlation, while the

12

predicted Nu-number by the GGDH and WET closures, agrees very well with the Dittus-Boelter correlation.

3.3 Rectangular Ducts

Different rectangular ducts (side ratio 2,3,5, and 10) are considered. Even in these cases, if the GGDH and WET models are used, both the friction factor and Nu-number predicted by the EASM agree very well with the theoretical correlations. If the SED model is used, the Nu-number is under-predicted by about 15%. In Fig. 9, the secondary flow motion for two rectangular ducts with aspect ratios of 3 and 5 are shown. The secondary motion velocity vectors predicted by the EASM, with the AKN damping functions in the $k - \varepsilon$ equations, are in good agreement with what has been observed in some experimental results. The existence of such secondary flow patterns was first observed by Nikuradse during his experiment with noncircular ducts (see Kakaç et al., 1987).
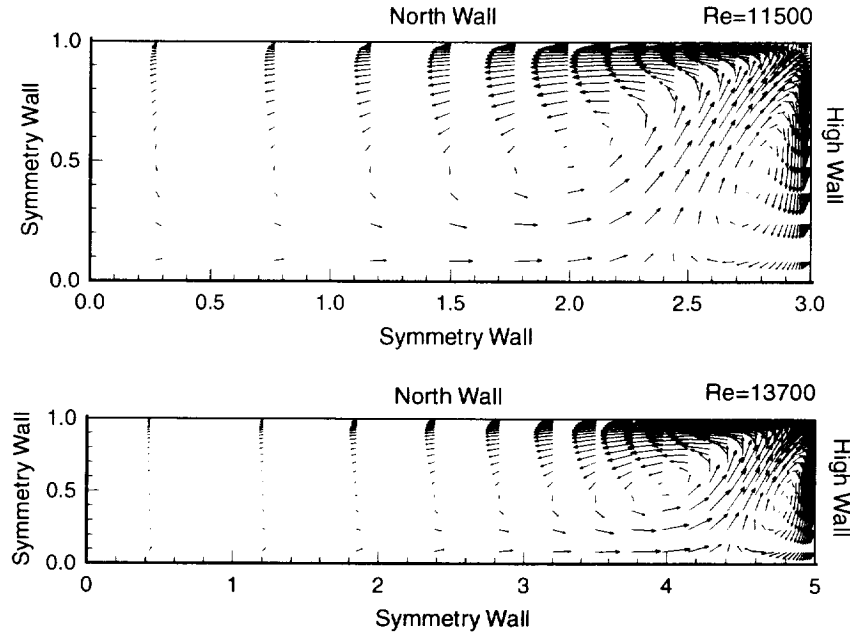

Figure 9. Predicted secondary motion velocity vectors in rectangular ducts with aspect ratios 3 and 5 using EASM with damping functions.

Table 2 provides calculated friction factor, Nu-number and the center-to-bulk-velocity ratio (U_c/U_b) in a rectangular duct with different aspect ratios. For a given cross section, the U_c/U_b decreases slightly with increasing Re number, which is also evident from this table. The experimental value of U_c/U_b for a rectangular duct with aspect ratio 8 at $Re \approx 5800$ is 1.23 (see Rokni et al., 1998) which can be compared with the calculation result (Table 2) 1.22 for aspect ratio 10 at $Re \approx 1.572 \times 10^4$.

Table 2. Calculated friction factor and Nu-number for rectangular ducts with different aspect ratios using EASM and GGDH.

Aspect Ratio	$Re \times 10^{-4}$	$f \times 10^3$	Nu	U_c/U_b
2	0.9397	8.165	30.4	1.28
3	1.1474	7.797	35.8	1.28
5	1.3666	7.541	41.2	1.27
10	1.5717	7.401	47.3	1.22

3.4 Trapezoidal and Triangular Ducts

The velocity vectors and the corresponding mean flow contours predicted by the EASM in a trapezoidal duct are presented in Fig. 10. As shown in the figure, there exist two counter rotating vortices close to each corner that are similar to the results obtained by Rokni and Sundén (1996). Only 61×31 grid points were used in the cross section to perform the calculation. Since the LB damping functions had convergence and stability problems regardless of grid arrangement in the cross section in the trapezoidal ducts, the AKN damping functions were used. In Fig. 10, the Re number is about 1.546×10^4, and the calculated friction factor and Nu-number (GGDH model) are 7.791×10^{-3} and 48.1, respectively. These values can be compared with the Prandtl-law and Dittus-Boelter correlations, Eqs. (17) and (19), which yield 6.900×10^{-3} and 46.8, respectively. The center-to-bulk-velocity ratio (U_c/U_b) is calculated as 1.29.

Close to the upper side corner ("north wall" and "high wall") there exist two counter-rotating vortices a small one and a much larger one. The smaller vortex size decreases when decreasing the upper side length ("north wall") until it vanishes for a triangular duct. Correspondingly, the large vortex size increases while this length decreases (see Fig. 11). This type of secondary flow pattern in a triangular duct was also observed in the experiment of Nikuradse (see e.g., Kakaç, 1987).

The highly stable nature of the calculation procedure used here makes it possible to apply the present models to such triangular ducts and to predict turbulence quantities without any convergence problems. In Fig. 11 the upper side length is much smaller than the two other lengths ($\approx 2 \times 10^{-3}$ of the duct height). This length cannot be set to zero since using structured grids in the calculations requires that no side of any control volume in the domain be zero. Nevertheless, this very small upper side length would still yield the correct limiting behavior of a sharp corner and would be a case in which many turbulence models would fail. The Re number in this duct is 1.164×10^4, and the predicted friction factor and Nu-number (GGDH model) are 8.016×10^{-3} and 36.3, respectively. These results can be compared with the Prandtl-law and Dittus-Boelter correlations, Eqs. (17) and (19), which yield 7.421×10^{-3} and 37.3, respectively. The center-to-bulk-velocity ratio (U_c/U_b) is calculated as 1.30.
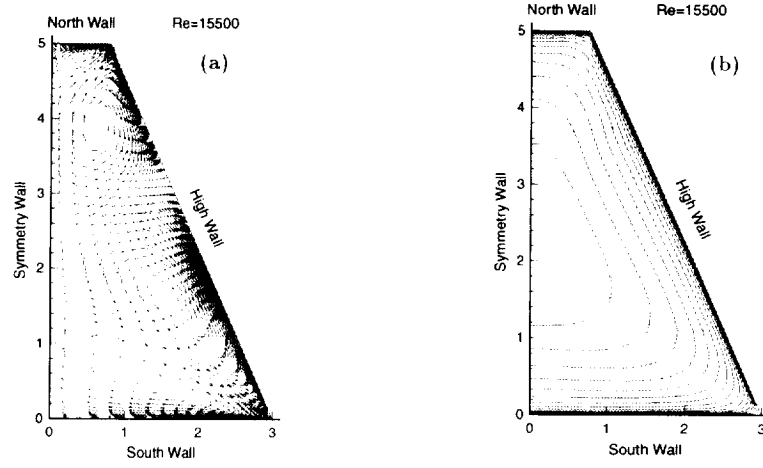
Figure 10. Velocity field in a trapezoidal duct: (a) secondary motion velocity vectors; (b) mean velocity contours.
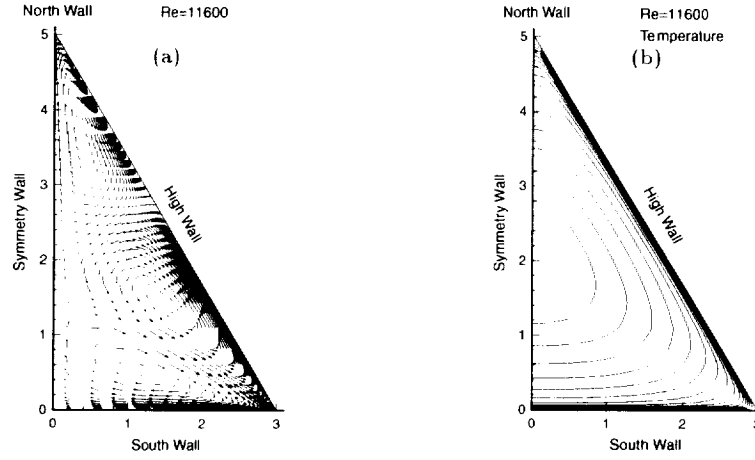

Figure 11. Predicted velocity and temperature fields in a triangular duct: (a) secondary motion velocity vectors; (b)mean temperature contours.

3.5 Wavy Ducts

In light of the success with the previous geometries, an initial calculation on a wavy duct has been done to further evaluate the performance of the model and calculation procedure presented in this study. The wavy duct under consideration is shown in Fig. 2. A symmetry plane is imposed at the cross section with an aspect ratio 4 to 3 and sinuous variation along the y-direction. The number of grid points in the cross section is set to 61×31 for y- and z-directions, respectively. This discretization is similar to the number and distribution of grid points used in the cross section for the trapezoidal duct. Close to each wall, the number of grid points, or control volumes, is increased to enhance the resolution and accuracy. Unfortunately, due to computer

15

capacity and time, only 30 grid points, uniformly spaced, are set in the streamwise, or x, direction.

For convergence, the residuals reached the value 10^{-4} for the temperature field and 10^{-5} for the velocity field and turbulence equations. The GGDH method was used for the temperature equation.

The restrictions on the streamwise resolution can adversely affect the performance of the solution procedure. Such inaccuracies in the computation in some regions may lead to large values of some key parameters which deteriorate the whole solution field. This situation occurs here, and to obtain a converged solution, restrictions are needed. The parameter $\mathcal{R}^2$ is a useful parameter for characterizing the flow. For a pure shear flow $\mathcal{R}^2 = 1$, and for a plain strain flow $\mathcal{R}^2 = 0$. In this study, the value being calculated in the cross section of the straight square duct was 0.947, for the trapezoidal duct, the value was 0.964, and for the triangular duct, the value was 0.958. This range of values suggests that the model will perform well since the EASM was originally calibrated for homogeneous shear flows where $\mathcal{R}^2 = 1$. In the wavy wall case, values of $\mathcal{R}^2$ exceeding 2 and correspondingly large values of η greater than 16 occur near the bend in the duct. These values yield too large values of P_k/ε, which eventually destroy the solution. Jongen and Gatski (1998) correlated the behavior of these three parameters $(\eta, \mathcal{R}^2, P_k/\varepsilon)$ (see their Fig. 4), and arrived at a limiting value for $\mathcal{R}$ given by

$$\mathcal{R}_{\text{lim}} = \pm \frac{1}{a_2} \sqrt{\frac{a_3^2}{3} + \frac{a_1}{g} \left(\frac{P_k}{\varepsilon} \right)^{-1}} \qquad (22)$$

The limiting value for $\mathcal{R}_{\text{lim}}$ was ± 1.23. At these points P_k/ε can be very large. Therefore, $\mathcal{R}_{\text{lim}}^2 = 1.513$ is the limiting value used in the calculations and this restricts the solution of the cubic equation, Eq. (9), to values of P_k/ε which do not lead to a deteriorated solution.

Table 3 shows the calculated Nu-number and friction factor for the wavy duct in comparison with the straight trapezoidal duct. Included in the table are columns where the calculated friction factor has been normalized by the Prandtl-law, and the calculated Nu-number has been normalized by the Dittus-Boelter correlation. As can

Table 3. Comparison between a wavy duct and straight duct with similar cross section.

Type	Re	$f \times 10^3$	$f_{\text{Pr}} \times 10^3$	f/f_{Pr}	GGDH	Nu_{DB}	Nu/Nu_{DB}
Straight	13699	7.466	7.115	1.05	40.4	42.5	0.95
Wavy	8944	17.527	7.956	2.20	48.2	30.2	1.60

be seen from Table 3, both the friction factor and the Nu-number for the wavy duct are much higher than the straight duct.

Figure 12 shows that the secondary velocity vectors at the inlet of the duct have changed significantly, compared to the straight duct. In addition, one can assume

16

that the secondary velocity patterns have also changed significantly in the other cross-section planes as well. The magnitude of these secondary flow patterns is about 10 times larger than the secondary flow in the straight duct with similar cross section, or about 10% of the streamwise flow. The contours in the streamwise flow direction
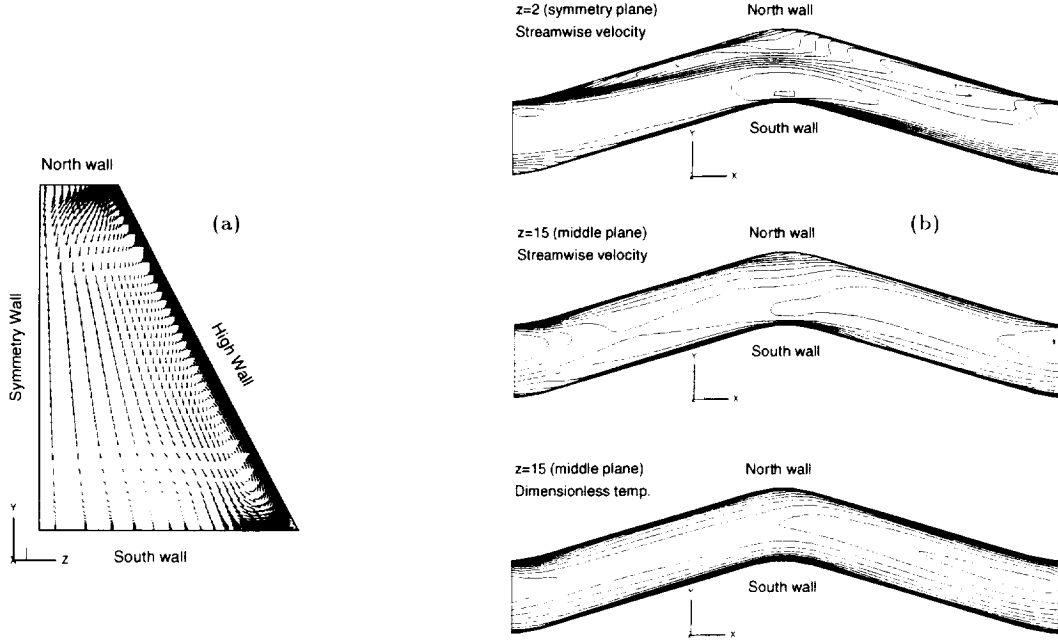

Figure 12. (a) Secondary motion velocity vectors at the inlet of the wavy duct, (b) streamwise velocity contours at symmetry and middle planes, and dimensionless temperature contours at middle plane of wavy duct.

are also shown in Fig. 12. The duct is moderately curved, and there is a very small recirculation zone in the streamwise symmetry plane of the duct near the north wall; however, no such recirculation exists in the middle plane. Such patterns suggest a complicated vortical flow field within the duct where components of vorticity in the cross-stream and streamwise directions may simultaneously exist.

4. Summary

The results from the numerical solution of fully developed, three-dimensional turbulent duct flow under isothermal conditions have been presented for square, rectangular, trapezoidal, triangular, and wavy ducts. The turbulent stresses were modeled using an EASM, and the turbulent heat fluxes were modeled by the SED, GGDH and WET methods. At high Reynolds numbers ($\gtrsim 10^5$), wall functions for the velocity and temperature fields were used. At low Reynolds numbers, the AKN damping functions were used for the turbulent equations, and for the turbulent heat fluxes (GGDH and WET methods), Lam-Bremhorst type damping functions were used. Compar-

isons with well-established correlations, extracted from experimental studies, showed excellent agreement for the hydraulic parametrs (friction factor and Nu-number). Qualitative comparisons with observed secondary flow patterns were also found to be in excellent agreement.

The calculation procedure was found to be robust, with limited demand on the total number of grid points to achieve the desired accuracy – thus minimizing the associated computational cost. This procedure included the very challenging triangular duct case, where excellent results were obtained without any convergence or stability problems. In the wavy duct with trapezoidal cross section, streamwise resolution problems necessitated the imposition of a limiting value on the characteristic flow parameter $\mathcal{R}$. Nevertheless, with this restriction, results were obtained showing the distinguishing features of the fully developed wavy duct flow as well as the contrasting behavior to the straight duct case with similar cross section.

These results suggest that while the models for the heat fluxes can be very simple, this simplicity does not necessarily preclude an accurate prediction of the temperature field. Under isothermal conditions, simple gradient-diffusion models for the heat fluxes may suffice if the flow field can be well predicted. In complex geometries such as those examined here, it is necessary to use higher-order models for the Reynolds stresses, since anisotropies in the turbulent stress field are important, and simple linear eddy viscosity models will not suffice. Higher-order closures for the heat fluxes may also be required in nonadiabatic cases and/or in cases where counter-gradient heat transfer occurs. Corresponding explicit algebraic heat flux models, coupled with equations for the temperature variance and variance dissipation rate, could be applied to such flows.

5. References

Abe, K.; Kondoh, T.; and Nagano, Y. 1995: A New Turbulence Model for Predicting Fluid Flow and Heat Transfer in Separating and Reattaching Flows-II. Thermal Field Calculations. *Int. J. Heat Mass Transfer*, Vol. **38**, pp. 1467–1481.

Gatski T. B.; and Speziale, C.G. 1993: On Explicit Algebraic Stress Models for Complex Turbulent Flows. *J. Fluid Mech.*, Vol. **254**, pp. 59–78.

Gavrilakis, S. 1992: Numerical Simulation of Low-Reynolds-number Turbulent Flow Through a Straight Square Duct. *J. Fluid Mech.*, Vol. **244**, pp. 101–129.

Huser, A.; and Biringen, S. 1993: Direct Numerical Simulation of Turbulent Flow in a Square Duct. *J. Fluid Mech.*, Vol. **257**, pp. 65–69.

Incropera F. P.; and DeWitt, D. P. 1996, *Fundamentals of Heat and Mass Transfer*, 4th ed. John Wiley & Sons.

Jayatilleke, C. V. 1969: The Influence of Prandtl Number and Surface Roughness on the Resistance of the Laminar Sublayer to Momentum and Heat Transfer. *Prog. Heat Mass Transfer*, Vol. **1**, pp. 193–329.

Jongen T.; and Gatski, T. B. 1998: A New Approach to Characterizing the Equilibrium States of the Reynolds Stress Anisotropy in Homogeneous Turbulence. *Theor. Comput. Fluid Dyn.*, **11**, 31–47. Erratum: *Theor. Comput. Fluid Dyn.*, **12**, 71–72.

Jongen, T.; and Gatski, T. B. 1999: A Unified Analysis of Planar Homogeneous Turbulence Using Single-Point Closure Equations. *J. Fluid Mech.*, Vol. **399**, pp. 117-150.

Kakaç, S.; Shah, R. K.; and Aung, W. 1987: *Handbook of Single-Phase Convective Heat Transfer*, John Wiley & Sons, pp. 4.73-4.83.

Kim, J.; Moin, P.; and Moser, R. 1987: Turbulence Statistics in Fully Developed Channel Flow at Low Reynolds Number. *J. Fluid Mech.*, Vol. **177**, pp. 133-166.

Lam, C. K. G.; and Bremhorst, K. 1981: A Modified Form of the $k - \varepsilon$ Model for Predicting Wall Turbulence. *ASME J. Fluid Engrg.*, Vol. **103**, pp. 456-460.

Launder, B. E. 1988: On the Computation of Convective Heat Transfer in Complex Turbulent Flows. *ASME J. Heat Transfer*, Vol. **110**, pp. 1112-1128.

Lowdermilk, W. H.; Wieland, W. F.; and Livingood, J. N. B. 1954: Measurements of Heat Transfer and Friction Coefficients for Flow of Air in Noncircular Ducts at High Surface Temperature. *NACA RN E53J07*.

Madabhushi, R. K.; and Vanka, S. P. 1991: Large Eddy Simulation of Turbulence-Driven Secondary Flow in a Square Duct. *Phys. Fluids A*, Vol. **3**, pp. 2734-2745.

Meyer, L.; and Rehme, K. 1994: Large-Scale Turbulence Phenomena in Compound Rectangular Channels. *Exp. Thermal Fluid Sci.*, Vol. **8**, pp. 286-304.

Mompean, G.; Gavrilakis, S.; Machiels, L.; and Deville, M. O. 1996: On Predicting the Turbulence-Induced Secondary Flows Using Non-Linear $k - \varepsilon$ Models. *Phys. Fluids*, Vol. **8**, pp. 1856-1868.

Rokni, M., 1998, *Numerical Investigation of Turbulent Fluid Flow and Heat Transfer in Complex Ducts*, Doctoral Thesis, ISSN 1104-7747, Div. of Heat Transfer, Lund Institute of Technology, Sweden.

Rokni, M.; and Sundén, B. 1996: A Numerical Investigation of Turbulent Forced Convection in Ducts With Rectangular and Trapezoidal Cross-Section Area by Using Different Turbulence Models. *Num. Heat Transfer*, Vol. **30**, pp. 321-346.

Rokni, M.; and Sundén, B. 1998: 3D Numerical Investigation of Turbulent Forced Convection In Wavy Ducts With Trapezoidal Cross Section. *Num. Meth. For Heat & Fluid Flow*, Vol. **8**, pp. 118-141.

Rokni, M.; and Sundén, B. 1999a: Performance of RNG Turbulence Modelling for Turbulent Forced Convective Heat Transfer in Ducts. *Int. J. Comp. Fluid Dyn.*, Vol. **11**, pp. 351-362.

Rokni, M.; and Sundén, B. 1999b: Improved Modelling of Turbulent Forced Convective Heat Transfer in Straight Ducts. *ASME J. Heat Trans.* Vol. **121**, pp. 712-719.

Rokni, M.; Olsson, C. O.; and Sundén, B. 1998: Numerical and Experimental Investigation of Turbulent Flow in Rectangular Ducts. *Int. J. Num. Meth. Fluids*, Vol. **28**, pp. 225-242.

Rumsey, C. L.; Gatski, T. B.; and Morrison, J. H. 1999: Turbulence Model Predictions of Extra-Strain Rate Effects in Strongly-Curved Flows. *AIAA 37th Aerospace Sciences Meeting & Exhibit*, Paper No. 99-0157.

Su, M. D.; and Friedrich, R. 1994: Investigation of Fully Developed Turbulent Flow In a Straight Duct With Large Eddy Simulation. *ASME J. Fluid Engrg.*, Vol. **116**, pp. 677-684.

REPORT DOCUMENTATION PAGE

Public reporting burden for this collection of information is estimated to average 1 hour per response, including the time for reviewing instructions, searching existing data sources, gathering and maintaining the data needed, and completing and reviewing the collection of information. Send comments regarding this burden estimate or any other aspect of this collection of information, including suggestions for reducing this burden, to Washington Headquarters Services, Directorate for Information Operations and Reports, 1215 Jefferson Davis Highway, Suite 1204, Arlington, VA 22202–4302, and to the Office of Management and Budget, Paperwork Reduction Project (0704–0188), Washington, DC 20503.

1. AGENCY USE ONLY *(Leave blank)*	2. REPORT DATE	3. REPORT TYPE AND DATES COVERED
	December 1999	Technical Memorandum

4. TITLE AND SUBTITLE
Predicting Turbulent Convective Heat Transfer in Three-Dimensional Duct Flows

5. FUNDING NUMBERS
522-31-11-03

6. AUTHOR(S)
M. Rokni and T. B. Gatski

7. PERFORMING ORGANIZATION NAME(S) AND ADDRESS(ES)
NASA Langley Research Center
Hampton, VA 23681–2199

8. PERFORMING ORGANIZATION REPORT NUMBER
L–17937

9. SPONSORING/MONITORING AGENCY NAME(S) AND ADDRESS(ES)
National Aeronautics and Space Administration
Washington, DC 20546–0001

10. SPONSORING/MONITORING AGENCY REPORT NUMBER
NASA/TM–1999–209843

11. SUPPLEMENTARY NOTES

12a. DISTRIBUTION/AVAILABILITY STATEMENT
Unclassified-Unlimited
Subject Category 34   Distribution: Nonstandard
Availability: NASA CASI (301) 621–0390

12b. DISTRIBUTION CODE

13. ABSTRACT *(Maximum 200 words)*
The performance of an explicit algebraic stress model is assessed in predicting the turbulent flow and forced heat transfer in straight ducts, with square, rectangular, trapezoidal and triangular cross-sections, under fully developed conditions over a range of Reynolds numbers. Iso-thermal conditions are imposed on the duct walls and the turbulent heat fluxes are modeled by gradient-diffusion type models. At high Reynolds numbers ($\gtrsim 10^5$), wall functions are used for the velocity and temperature fields; while at low Reynolds numbers damping functions are introduced into the models. Hydraulic parameters such as friction factor and Nusselt number are well predicted even when damping functions are used, and the present formulation imposes minimal demand on the number of grid points without any convergence or stability problems. Comparison between the models is presented in terms of the hydraulic parameters, friction factor and Nusselt number, as well as the secondary flow patterns occurring within the ducts.

14. SUBJECT TERMS
Turbulence Modeling, Turbulent Heat Transfer, Turbulent Duct Flows

15. NUMBER OF PAGES
24

16. PRICE CODE
A03

17. SECURITY CLASSIFICATION OF REPORT	18. SECURITY CLASSIFICATION OF THIS PAGE	19. SECURITY CLASSIFICATION OF ABSTRACT	20. LIMITATION OF ABSTRACT
Unclassified	Unclassified	Unclassified	

NSN 7540-01-280-5500